Low Densities Instability of Relativistic Mean Field Models

A. Sulaksono and T. Mart

Departemen Fisika, FMIPA, Universitas Indonesia, Depok, 16424, Indonesia

Abstract

The effects of the symmetry energy softening of the relativistic mean field (RMF) models on the properties of matter with neutrino trapping are investigated. It is found that the effects are less significant than those in the case without neutrino trapping. The weak dependence of the equation of state on the symmetry energy is shown as the main reason of this finding. Using different RMF models the dynamical instabilities of uniform matters, with and without neutrino trapping, have been also studied. The interplay between the dominant contribution of the variation of matter composition and the role of effective masses of mesons and nucleons leads to higher critical densities for matter with neutrino trapping. Furthermore, the predicted critical density is insensitive to the number of trapped neutrinos as well as to the RMF model used in the investigation. It is also found that additional nonlinear terms in the Horowitz-Piekarewicz and Furnstahl-Serot-Tang models prevent another kind of instability, which occurs at relatively high densities. The reason is that the effective σ meson mass in their models increases as a function of the matter density.

I. INTRODUCTION

Recently, the dynamical stability of the uniform ground state of multi components systems (i.e., electrons, protons, and neutrons) at low densities has received considerable attentions [1, 2, 3, 4, 5, 6]. This interest is motivated by the fact that the neutron star is expected to have a solid inner crust of nonuniform neutron-rich matter above its liquid mantle [3] and the mass of its crust depends sensitively on the density of its inner edge and on its equation of state (EOS) [2]. Meanwhile, the critical density (ρ_c), a density at which the uniform liquid becomes unstable to a small density fluctuation, can be used as a good approximation of the edge density of the crust [3]. Using the Skyrme SLy effective interactions, Ref. [2] found the inner edge of the crust density to be $\rho_{\text{edge}} = 0.08$ fm^{-3}. Reference [3] generalized the dynamical stability analysis of Ref. [7] in order to accommodate the various nonlinear terms in the relativistic mean field (RMF) model of Horowitz-Piekarewicz [4]. They found a strong correlation between ρ_c in neutron star and the symmetry energy (a_{sym}) which leads to a linear relation between ρ_c and the skin thickness of finite nuclei.

These results suggested that a measurement of the neutron radius in ^{208}Pb will provide useful information on the ρ_c [3, 4]. Recently, a new version of the RMF model based on effective field theory (ERMF) has been proposed by Furnstahl, Serot, and Tang [8]. The predictive power of the model in a wide range of densities is quite impressive (see the review articles [9, 10] for the details). On the other hand, an adjustment of the isovector-vector channel of the ERMF model in order to achieve a softer density dependence of a_{sym} at high densities has been done in Ref. [11].

Similar to the previous calculation done in [4], but using a different RMF model, it is found that by adjusting that channel a lower proton fraction (Y_p) in high density neutron star matter can be achieved without significantly changing the bulk properties [11]. It is well known that Y_p is related to the threshold of the direct URCA cooling process and the trend of the density distribution of Y_p is unique for each model which is sensitive to the different forms of nonlinear terms used. Therefore, an investigation of the EOS and the instability at low densities by using different RMF models could be quite interesting. Indeed, by comparing our results with the previous ones [3, 4], we can systematically study the influence of the form and the strength of isovector-vector nonlinear terms on the critical density. The presence of electrons and the influence of the electromagnetic interaction on

the unstable modes of asymmetric matter as well as the comparison between dynamical instability region with the thermodynamical one have been investigated in Refs. [5, 6] by using the standard RMF model within the Vlasov formalism. They observed the important role of the Coulomb field in the large structure formation and also the role of the electron dynamics in restoring the large-wavelength instabilities [6].

In the actual situation, muons may also be present in the stellar matters. Their existence yields an additional electromagnetic contribution besides the electrons and protons ones. The significance of their contribution depends on the matter composition. Including muons in the dynamical instability analysis of uniform matter increases the electromagnetic effect on the ρ_c in medium. Moreover, in supernovae or protoneutron stars neutrinos can be trapped inside, if their mean free paths are smaller than the star radius. In general, the presence of trapped neutrinos in matter affects the stiffness of EOS and drastically changes the composition of neutral matter [12, 13, 14, 15, 16]. It was also found that neutrino trapping causes the strange baryon [12, 13] and kaon condensate [12, 14] to appear at higher densities as compared to the case without neutrino trapping. In Ref. [16], the EOS of the strangeness rich protoneutron star and the EOS of neutron star matter with temperature different from zero have been already studied by means of the ERMF model. Meanwhile, like neutron stars, protoneutron stars have dense cores and outer layers [16] and in supernovae inhomogeneity can appear below the saturation density of nuclear matter (ρ_0) [17, 18]. Therefore, an investigation of the boundary between the two phases, which leads to the determination of ρ_c, becomes crucial for a realistic and complete description of stellar matters.

In the present work, we shall extend the analysis of dynamical stability in uniform matter of Ref. [3] in two ways, i.e., first, we consider the muon contribution and, second, we shall consider all possible mixings of vector and isovector contributions caused by the nonlinear terms in the ERMF model. The parameter set NL3 of the standard RMF [19] model as well as the parameter sets Z271 and Z271* of the Horowitz-Piekarewicz one [4] will be presented for comparison. The results are used to study the effect of the neutrino presence on the ρ_c values. Here, we only use nucleons in the baryonic sector along with σ, ω, and ρ mesons in the mesonic sector because ρ_c usually appears at a density lower than ρ_0 and the strange particles appear at a density higher than $2\rho_0$. Furthermore, in the neutrino trapping case they appear at higher density than in the case without neutrino trapping. Therefore, we can assume the strange particles to have only minor effects on the ρ_c and, as a consequence,

their contributions may be neglected in this work. On the other hand, although in the real situation the temperature of protoneutron stars is not equal to zero and the supernovae inner core can have a temperature around $T \sim (10\text{-}50)$ MeV, the zero temperature approximation can be assumed here since the temperature effect on the EOS of supernovae matter and on the maximum mass of protoneutron star [14, 15] is smaller than that without neutrino trapping. In this approximation, the following constraints can be used to calculate the fraction of every constituent in matter:

- balance equation for the chemical potentials

$$\mu_n + \mu_{\nu_e} = \mu_p + \mu_e, \tag{1}$$

- conservation of the charge neutrality

$$\rho_e + \rho_\mu = \rho_p, \tag{2}$$

where the total density of baryon is given by

$$\rho_B = \rho_n + \rho_p, \tag{3}$$

while the fixed electronic-leptonic fraction Y_{l_e} is defined as

$$Y_{l_e} = \frac{\rho_e + \rho_{\nu_e}}{\rho_B} \equiv Y_e + Y_{\nu_e}, \tag{4}$$

where Y_{ν_e} and Y_e are neutrino electron and electron fractions, respectively. In addition, we will revisit the EOS of matter with neutrino trapping because we want to study the effect of different adjustments in the isovector-vector sector [11] on the EOS of matter with neutrino trapping. They were not fully explored in our previous works [11, 20].

This paper is organized as follows. In Sec. II, a brief review of the model is given. Calculation of the dielectric function is presented in Sec. III, while numerical results along with the corresponding discussions are given in Sec. IV. Finally, we give the conclusion in Sec. V.

II.   RELATIVISTIC MEAN FIELD MODELS

Our starting point to describe the non-strange dense stellar matter is an effective Lagrangian density for interacting nucleons, σ, ω, ρ mesons as well as noninteracting leptons.

The Lagrangian density for standard RMF models can be found in Refs. [10, 21, 22]. We note that in order to modify the density dependence of a_{sym}, Horowitz-Piekarewicz have recently added isovector-vector nonlinear terms ($\mathcal{L}_{\text{HP}}$) in a standard RMF model [4]. In the case of ERMF model, the corresponding Lagrangian density can be found in Refs. [8, 11, 23]. For the convenience of the reader, we write the Lagrangian density in a compact form as

$$\mathcal{L} = \mathcal{L}_N + \mathcal{L}_M + \mathcal{L}_{\text{HP}} + \mathcal{L}_L, \tag{5}$$

where the nucleon part, up to order $\nu = 3$, reads

$$\begin{aligned}
\mathcal{L}_N &= \bar{\psi}[i\gamma^\mu(\partial_\mu + i\bar{\nu}_\mu + ig_\rho\bar{b}_\mu + ig_\omega V_\mu) + g_A\gamma^\mu\gamma^5\bar{a}_\mu \\
&\quad - M + g_\sigma\sigma]\psi - \frac{f_\rho g_\rho}{4M}\bar{\psi}\bar{b}_{\mu\nu}\sigma^{\mu\nu}\psi,
\end{aligned} \tag{6}$$

with

$$\psi = \begin{pmatrix} p \\ n \end{pmatrix}, \quad \bar{\nu}_\mu = -\frac{i}{2}(\bar{\xi}^\dagger\partial_\mu\bar{\xi} + \bar{\xi}\partial_\mu\bar{\xi}^\dagger) = \bar{\nu}_\mu^\dagger, \tag{7}$$

$$\bar{a}_\mu = -\frac{i}{2}(\bar{\xi}^\dagger\partial_\mu\bar{\xi} - \bar{\xi}\partial_\mu\bar{\xi}^\dagger) = \bar{a}_\mu^\dagger, \tag{8}$$

$$\bar{\xi} = \exp(i\bar{\pi}(x)/f_\pi), \quad \bar{\pi}(x) = \frac{1}{2}\vec{\tau} \cdot \vec{\pi}(x), \tag{9}$$

$$\bar{\pi}(x) = \frac{1}{2}\vec{\tau} \cdot \vec{\pi}(x), \tag{10}$$

$$\bar{b}_{\mu\nu} = D_\mu\bar{b}_\nu - D_\nu\bar{b}_\mu + ig_\rho[\bar{b}_\mu, \bar{b}_\nu], \quad D_\mu = \partial_\mu + i\bar{\nu}_\mu, \tag{11}$$

$$V_{\mu\nu} = \partial_\mu V_\nu - \partial_\nu V_\mu, \tag{12}$$

$$\sigma^{\mu\nu} = \frac{1}{2}[\gamma^\mu, \gamma^\nu]. \tag{13}$$

where, p and n are the proton and neutron fields, M is the nucleon mass, while σ, $\vec{\pi}$, V^μ, and $\vec{b}^\mu$ are the σ, π, ω and ρ meson fields, respectively. The meson contribution, up to order

$\nu = 4$ is

$$\begin{aligned}
\mathcal{L}_M &= \frac{1}{4}f_\pi^2\mathrm{Tr}(\partial_\mu\bar{U}\partial^\mu\bar{U}^\dagger) + \frac{1}{4}f_\pi^2\mathrm{Tr}(\bar{U}\bar{U}^\dagger - 2) + \frac{1}{2}\partial_\mu\sigma\partial^\mu\sigma \\
&\quad - \frac{1}{2}\mathrm{Tr}(\bar{b}_{\mu\nu}\bar{b}^{\mu\nu}) - \frac{1}{4}V_{\mu\nu}V^{\mu\nu} - g_{\rho\pi\pi}\frac{2f_\pi^2}{m_\rho^2}\mathrm{Tr}(\bar{b}_{\mu\nu}\bar{\nu}^{\mu\nu}) \\
&\quad + \frac{1}{2}\left(1 + \eta_1\frac{g_\sigma\sigma}{M} + \frac{\eta_2}{2}\frac{g_\sigma^2\sigma^2}{M^2}\right)m_\omega^2 V_\mu V^\mu + \frac{1}{4!}\zeta_0 g_\omega^2(V_\mu V^\mu)^2 \\
&\quad + \left(1 + \eta_\rho\frac{g_\sigma\sigma}{M}\right)m_\rho^2\mathrm{Tr}(\bar{b}_\mu\bar{b}^\mu) - m_\sigma^2\sigma^2\left(1 + \frac{\kappa_3}{3!}\frac{g_\sigma\sigma}{M} + \frac{\kappa_4}{4!}\frac{g_\sigma^2\sigma^2}{M^2}\right),
\end{aligned} \tag{14}$$

where

$$\bar{U} = \bar{\xi}^2, \qquad \bar{\nu}_{\mu\nu} = \partial_\mu\bar{\nu}_\nu - \partial_\nu\bar{\nu}_\mu + i[\bar{\nu}_\mu, \bar{\nu}_\nu] = -i[\bar{a}_\mu, \bar{a}_\nu]. \tag{15}$$

In the mean field approximation, π meson does not contribute. In the Horowitz-Piekarewicz model [4] the isovector-vector nonlinear term reads

$$\mathcal{L}_{\mathrm{HP}} = 4\Lambda_V g_\rho^2 g_\omega^2 \, \vec{b}^\mu \cdot \vec{b}_\mu \, V^\mu V_\mu. \tag{16}$$

We note that changing the g_ρ and Λ_V parameters in the Horowitz-Piekarewicz model [4], or g_ρ and η_ρ parameters in the ERMF model [11], affects the density dependent part of the a_{sym}. A more detailed procedure to adjust the density dependence of the nuclear matter symmetry energy in RMF models can be found in Refs. [4, 11, 24].

For the leptons, the free Lagrangian density

$$\mathcal{L}_L = \sum_{l=e^-, \ \mu^-, \ \nu_e, \ \nu_\mu} \bar{l}(\gamma^\mu\partial_\mu - m_l)l, \tag{17}$$

is used. In the present work, the following parameter sets are chosen:

- Standard RMF model: NL3 [19],

- Standard RMF model plus isovector-vector nonlinear term: Z271 and Z271* [4],

- ERMF models: G2 [8] and G2* [11].

The coupling constants for all parameter sets are shown in Table I.

TABLE I: Numerical values of the coupling constants used in the parameter sets.

Parameter	G2	NL3	G2*	Z271	Z271*
m_σ/M	0.554	0.541	0.554	0.495	0.495
$g_\sigma/(4\pi)$	0.835	0.813	0.835	0.560	0.560
$g_\omega/(4\pi)$	1.016	1.024	1.016	0.670	0.670
$g_\rho/(4\pi)$	0.755	0.712	0.938	0.792	0.916
κ_3	3.247	1.465	3.247	1.325	1.325
κ_4	0.632	-5.668	0.632	31.522	31.522
ζ_0	2.642	0	2.642	4.241	4.241
η_1	0.650	0	0.650	0	0
η_2	0.110	0	0.110	0	0
η_ρ	0.390	0	4.490	0	0
Λ_V	0	0	0	0	0.03

III.   DYNAMICAL INSTABILITY OF UNIFORM DENSE STELLAR MATTERS

In order to accommodate muons and various nonlinear terms in the ERMF model, we have to extend the stability analyses of the uniform ground state of Refs. [3, 7, 27]. To that end, the longitudinal polarization matrix in these analyses is modified as follows

$$\Pi_L = \begin{pmatrix} \Pi_{00}^e & 0 & 0 & 0 & 0 \\ 0 & \Pi_{00}^\mu & 0 & 0 & 0 \\ 0 & 0 & \Pi_s & \Pi_m^p & \Pi_m^n \\ 0 & 0 & \Pi_m^p & \Pi_{00}^p & 0 \\ 0 & 0 & \Pi_m^n & 0 & \Pi_{00}^n \end{pmatrix}, \tag{18}$$

where the scalar polarization $\Pi_s = \Pi_s^p + \Pi_s^n$. In Eq. (18), the polarization due to the mixing between scalar and vector terms through sigma meson is indicated by Π_m. In the limit of $q_0 \to 0$, the individual polarization components are [3]

$$\begin{aligned} \Pi_s(q,0) = & \frac{1}{2\pi^2}\left\{ k_F E_F - \left(3M^{*\,2} + \frac{q^2}{2} \right) \ln\frac{k_F + E_F}{M^*} \right. \\ & \left. + \frac{2E_F E^2}{q}\ln\left|\frac{2k_F - q}{2k_F + q}\right| - \frac{2E^3}{q}\ln\left|\frac{qE_F - 2k_F E}{qE_F + 2k_F E}\right| \right\}, \end{aligned} \tag{19}$$

for the scalar polarization,

$$\Pi_m(q,0) = \frac{M^*}{2\pi^2}\left\{k_F - \left(\frac{k_F^2}{q} - \frac{q}{4}\right)\ln\left|\frac{2k_F - q}{2k_F + q}\right|\right\}, \tag{20}$$

for the mixed scalar-vector polarization, and

$$\begin{aligned}
\Pi_{00}(q,0) = & -\frac{1}{\pi^2}\left\{\frac{2}{3}k_F E_F - \frac{q^2}{6}\ln\frac{k_F + E_F}{M^*} - \frac{E_F}{3q}\left(M^{*\,2} + k_F^2 - \frac{3q^2}{4}\right)\ln\left|\frac{2k_F - q}{2k_F + q}\right|\right. \\
& \left. + \frac{E}{3q}\left(M^{*\,2} - \frac{q^2}{2}\right)\ln\left|\frac{qE_F - 2k_F E}{qE_F + 2k_F E}\right|\right\},
\end{aligned} \tag{21}$$

for the longitudinal polarization, with Fermi momentum k_F, nucleon effective mass $M^* = M - g_\sigma\sigma$, Fermi energy $E_F = (k_F^2 + M^{*\,2})^{1/2}$ and $E = (q^2/4 + M^{*\,2})^{1/2}$. For electron (e) or muon (μ), M^* is equal to electron or muon mass, respectively.

The longitudinal meson propagator now reads

$$D_L = \begin{pmatrix}
d_g & d_g & 0 & -d_g & 0 \\
d_g & d_g & 0 & -d_g & 0 \\
0 & 0 & -d_s & d_{sv\rho}^+ & d_{sv\rho}^- \\
-d_g & -d_g & d_{sv\rho}^+ & d_{33} & d_{v\rho}^- \\
0 & 0 & d_{sv\rho}^- & d_{v\rho}^- & d_{44}
\end{pmatrix}, \tag{22}$$

where $d_{sv\rho}^+ = -(d_{sv} + d_{s\rho})$, $d_{sv\rho}^- = -(d_{sv} - d_{s\rho})$, $d_{v\rho}^- = d_v - d_\rho$, $d_{33} = d_g + d_v + d_\rho + 2d_{v\rho}$ and $d_{44} = d_v + d_\rho - 2d_{v\rho}$. In this form, mixing propagators between isoscalar-scalar and isoscalar-vector (d_{sv}), isoscalar-vector and isovector-vector $(d_{v\rho})$, isoscalar-scalar and isovector-vector $(d_{s\rho})$ are present due to the nonlinear terms in the model, in addition to the standard photon, omega, sigma and rho propagators $(d_g, d_v, d_s$ and $d_\rho)$. These propagators are determined from the quadratic fluctuations around the static solutions which are generated by the second derivatives of energy density $(\partial^2\epsilon/\partial\phi_i\partial\phi_j)$, where ϕ_i and ϕ_j are the involved meson fields. The energy density ϵ derived from Eq. (5) reads

$$\begin{aligned}
\epsilon = & \frac{2}{(2\pi)^3}\sum_{i=p,n,e,\mu,\nu_e,\nu_\mu}\int d^3k_i E_i(k_i) + g_\omega V_0(\rho_p + \rho_n) + \frac{1}{2}g_\rho b_0(\rho_p - \rho_n) \\
& - \frac{1}{4}c_3 V_0^4 - \frac{1}{2}m_\omega^2 V_0^2 - d_2\sigma V_0^2 - \frac{1}{2}d_3\sigma^2 V_0^2 \\
& + \frac{1}{2}m_\sigma^2\sigma^2 + \frac{1}{3}b_2\sigma^3 + \frac{1}{4}b_3\sigma^4 \\
& - \frac{1}{2}m_\rho^2 b_0^2 - f_2\sigma b_0^2 - \frac{1}{2}\tilde{\Lambda}_s b_0^2\sigma^2 - \frac{1}{2}\tilde{\Lambda}_v b_0^2 V_0^2.
\end{aligned} \tag{23}$$

From Eq. (23) we can obtain the explicit form of all contributions to the longitudinal propagator. Note that the energy density of the ERMF model can be obtained from Eq. (23) by using the following explicit expressions of the coupling constants:

$$b_2 = \frac{g_\sigma \kappa_3 m_\sigma^2}{2M}, \quad b_3 = \frac{g_\sigma^2 \kappa_4 m_\sigma^2}{6M^2}, \quad f_2 = \frac{g_\sigma \eta_\rho m_\rho^2}{2M},$$
$$d_2 = \frac{g_\sigma \eta_1 m_\omega^2}{2M}, \quad d_3 = \frac{g_\sigma^2 \eta_2 m_\omega^2}{2M^2}, \quad c_3 = \frac{g_\omega^2 \xi_0}{6},$$
$$\tilde{\Lambda}_s = \tilde{\Lambda}_v = 0. \tag{24}$$

On the other hand, if we set the coupling constants in Eq. (23) to

$$f_2 = d_2 = d_3 = 0, \quad \tilde{\Lambda}_s = 2\Lambda_s g_\rho^2 g_\sigma^2, \quad \tilde{\Lambda}_v = 2\Lambda_v g_\rho^2 g_\omega^2, \tag{25}$$

we will obtain the energy density of the Horowitz-Piekarewicz model [4]. The mesons effective masses and the mixing polarizations calculated from the energy density [Eq. (23)] are given by

$$m_\sigma^{*\,2} = \frac{\partial^2 \epsilon}{\partial^2 \sigma} = m_\sigma^2 + 2b_2\sigma + 3b_3\sigma^2 - d_3 V_0^2 - \tilde{\Lambda}_s b_0^2,$$
$$m_\omega^{*\,2} = -\frac{\partial^2 \epsilon}{\partial^2 V_0} = m_\omega^2 + 2d_2\sigma + d_3\sigma^2 + 3c_3 V_0^2 + \tilde{\Lambda}_v b_0^2,$$
$$m_\rho^{*\,2} = -\frac{\partial^2 \epsilon}{\partial^2 b_0} = m_\rho^2 + 2f_2\sigma + \tilde{\Lambda}_s \sigma^2 + \tilde{\Lambda}_v V_0^2,$$
$$\tag{26}$$

and

$$\Pi_{\sigma\omega}^0 = -\frac{\partial^2 \epsilon}{\partial\sigma\partial V_0} = 2d_2 V_0 + 2d_3\sigma V_0,$$
$$\Pi_{\sigma\rho}^0 = -\frac{\partial^2 \epsilon}{\partial\sigma\partial b_0} = 2f_2 b_0 + 2\tilde{\Lambda}_s \sigma b_0,$$
$$\Pi_{\omega\rho}^{00} = \frac{\partial^2 \epsilon}{\partial V_0 \partial b_0} = -2\tilde{\Lambda}_v V_0 b_0. \tag{27}$$

By substituting Eqs. (26) and (27) in the σ, ω, and ρ propagators,

$$d_s = \frac{g_\sigma^2 (q^2 + m_\omega^{*\,2})(q^2 + m_\rho^{*\,2})}{(q^2 + m_\omega^{*\,2})(q^2 + m_\rho^{*\,2})(q^2 + m_\sigma^{*\,2}) + (\Pi_{\sigma\omega}^0)^2 (q^2 + m_\rho^{*\,2}) + (\Pi_{\sigma\rho}^0)^2 (q^2 + m_\omega^{*\,2})}, \tag{28}$$

$$d_v = \frac{g_\omega^2 (q^2 + m_\sigma^{*\,2})(q^2 + m_\rho^{*\,2})}{(q^2 + m_\omega^{*\,2})(q^2 + m_\rho^{*\,2})(q^2 + m_\sigma^{*\,2}) + (\Pi_{\sigma\omega}^0)^2 (q^2 + m_\rho^{*\,2}) - (\Pi_{\omega\rho}^{00})^2 (q^2 + m_\sigma^{*\,2})}, \tag{29}$$

9

$$d_\rho = \frac{1/4 g_\rho^2 (q^2 + m_\sigma^{*\,2})(q^2 + m_\omega^{*\,2})}{(q^2 + m_\omega^{*\,2})(q^2 + m_\rho^{*\,2})(q^2 + m_\sigma^{*\,2}) + (\Pi_{\sigma\rho}^0)^2 (q^2 + m_\omega^{*\,2}) - (\Pi_{\omega\rho}^{00})^2 (q^2 + m_\sigma^{*\,2})}, \quad (30)$$

and in the mixing propagators,

$$d_{sv} = \frac{g_\sigma g_\omega \Pi_{\omega\sigma}^0 (q^2 + m_\rho^{*\,2})}{H(q, q_0 = 0)}, \quad (31)$$

$$d_{s\rho} = \frac{1/2 g_\rho g_\sigma \Pi_{\sigma\rho}^0 (q^2 + m_\omega^{*\,2})}{H(q, q_0 = 0)}, \quad (32)$$

$$d_{v\rho} = \frac{1/2 g_\rho g_\omega \Pi_{\omega\rho}^{00} (q^2 + m_\sigma^{*\,2})}{H(q, q_0 = 0)}, \quad (33)$$

with

$$\begin{aligned} H(q, q_0 = 0) &= (q^2 + m_\omega^{*\,2})(q^2 + m_\rho^{*\,2})(q^2 + m_\sigma^{*\,2}) + (\Pi_{\sigma\omega}^0)^2 (q^2 + m_\rho^{*\,2}) \\ &+ (\Pi_{\sigma\rho}^0)^2 (q^2 + m_\omega^{*\,2}) - (\Pi_{\omega\rho}^{00})^2 (q^2 + m_\sigma^{*\,2}), \end{aligned} \quad (34)$$

and photon's propagator

$$d_g = \frac{e^2}{q^2}, \quad (35)$$

and using the explicit form of each component, the longitudinal meson propagator can be obtained.

The explicit derivation of each propagator is given in Appendix A. Note that by setting all coupling constants in Eqs. (28) - (33) which are not required by the Horowitz-Piekarewicz model [4] to zero, Eqs. (8), (13) - (14) of Ref. [3] can be obtained.

The uniform ground state system becomes unstable to small-amplitude density fluctuations with momentum transfer q when the following condition is satisfied [3]

$$\det\left[1 - D_L(q)\Pi_L(q, q_0 = 0)\right] \le 0. \quad (36)$$

The explicit form of Eq. (36) is given in Appendix B. In the case that the density is smaller than ρ_0, the critical density ρ_c is the largest density for which Eq. (36) has a solution. In the case that the density is larger than ρ_0, if any, ρ_c is the smallest density.
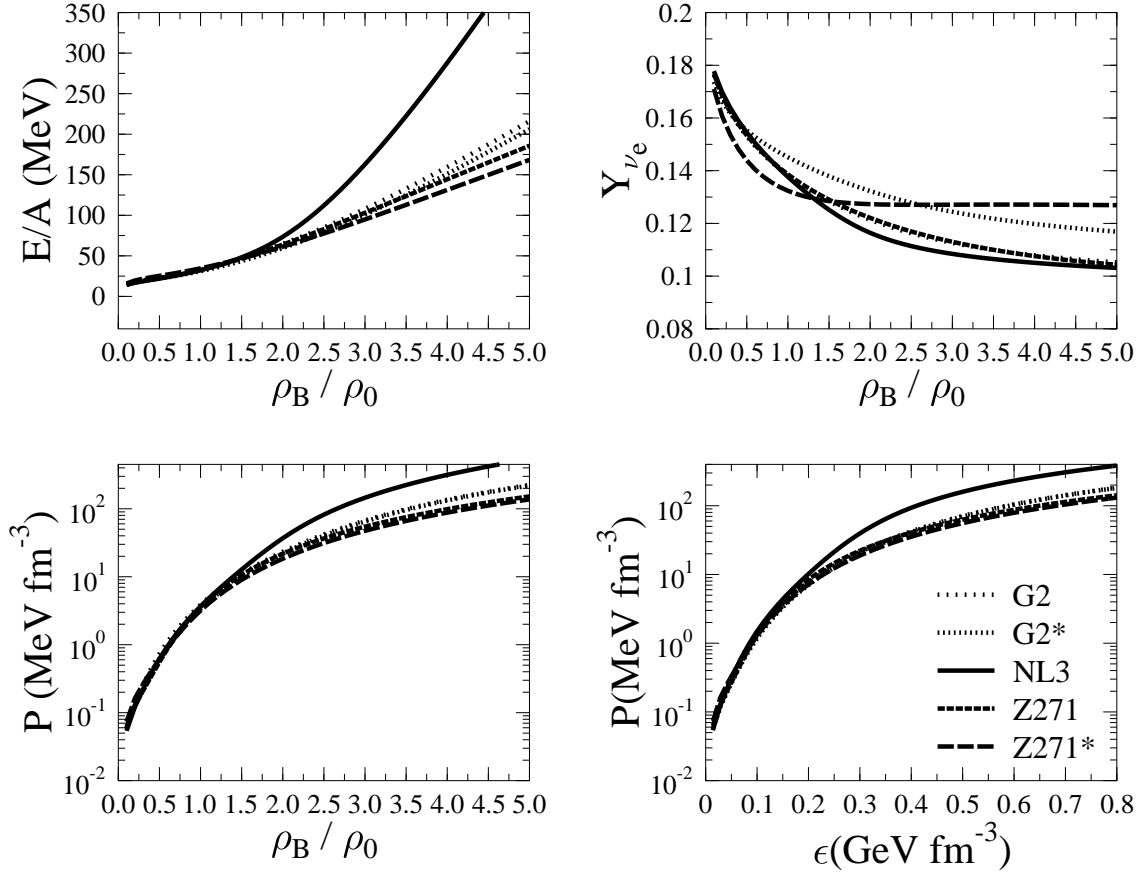
FIG. 1: Binding energy per nucleon (upper left panel) and the neutrino electron fraction (upper right panel) as a function of the baryon density, as well as the equation of states (EOS) as functions of baryon density (lower left panel) and energy density (lower right panel) according to RMF models. The curves are obtained by using $Y_{l_e} = 0.3$.

IV. NUMERICAL RESULTS AND DISCUSSIONS

Before discussing the dynamical instability of non-strange dense stellar matter, we will discuss the effects of different treatments in the isovector-vector sector [11] on the EOS, binding energies (E/A) and the neutrino electron fraction (Y_{ν_e}) of matter with neutrino trapping. The results are shown in Fig. 1. In contrast to the case of matter without neutrino trapping [11], significant differences in the trends of E/A and EOS start to appear at $\rho_B/\rho_0 \approx 2.0$. Except at sufficiently high densities, the difference between G2 and G2*, or Z271 and Z271*, does not significantly show up in these trends. These results can be understood from the asymmetry expansion of the binding energy of the corresponding matter

11

in the vicinity of the symmetric nuclear matter (SNM). The latter is given by [24, 25, 26]

$$E/A(\rho_B, \alpha) = (E/A)_{\text{SNM}}(\rho_B, \alpha) + \underbrace{\alpha^2 a_{\text{sym}}(\rho_B)}_{\Delta E_1/A(\rho_B, \alpha)} + \underbrace{O(\alpha^4)}_{\Delta E_2/A(\rho_B, \alpha)} + \Delta E_L/A(\rho_B), \qquad (37)$$

where $\alpha = Y_N - Y_P$ and $\Delta E_L/A$ is the electrons and muons contribution to the binding energy. We have found that for all parameter sets and matters used the value of $\Delta E_L/A$ is smaller than the other terms. The $\Delta E_2/A$ term is given by [26]

$$\Delta E_2/A(\rho_B, \alpha) = \alpha^4 Q(\rho_B) + ... \qquad (38)$$

The origin and connection of the quartic term $[Q(\rho_B)]$ to direct URCA are discussed in Ref. [26]. For the case of pure neutron matter ($\Delta E_1/A = a_{\text{sym}}$) or other fixed α cases it is known that $\Delta E_2 \ll \Delta E_1$. This means that the convergence of the expansion is considerably fast for these asymmetric matters but for matter with and without neutrino trapping the situation is quite different (see Fig. 2). We can see that by imposing the neutrality and β stability conditions on the matter with and without neutrino trapping, the corresponding asymmetry (α) becomes density dependent and, evidently, their $\Delta E_2/A$ are substantially larger compared to that of the PNM, for example. This indicates that in these cases, the convergence is significantly slow or even can not be reached at all. Additional constraint in the form of fixed electronic lepton fraction (Y_{l_e}) for the case of matter with neutrino trapping causes the decrease of α^2 and the convergence of binding energy expansion are slower than those in neutrinoless matter.

In Fig. 3 we show the $\Delta E_2/A$ and $\Delta E_1/A$ as a function of the ratio between baryon and nuclear saturation densities for the matter with and without neutrino trapping where G2, G2*, Z271, Z271* and NL3 parameter sets are used. The difference between the two types of matters appears mainly at densities lower than $2\rho_0$, where $\Delta E_2/A$ is smaller than $\Delta E_1/A$ for neutrinoless matter. The opposite situation happens for the neutrino trapping case. In the case of neutrinoless matter and parameter sets with a stiff a_{sym}, $\Delta E_2/A$ is larger than $\Delta E_1/A$ for the density larger than $2\rho_0$, but for the case of soft a_{sym} this condition is reached only after the density becomes relatively high. Figure 4 shows the characteristic of α^2 for both matters as the baryon density increases. Here, the dependence of α^2 on parameter sets is obvious for matter without neutrino trapping, while the opposite situation happens for matter with neutrino trapping. The symmetry energy is shown in Fig. 5, where we can clearly see its dependence on the parameter sets. The dependency of $\Delta E_2/A$, $\Delta E_1/A$ and
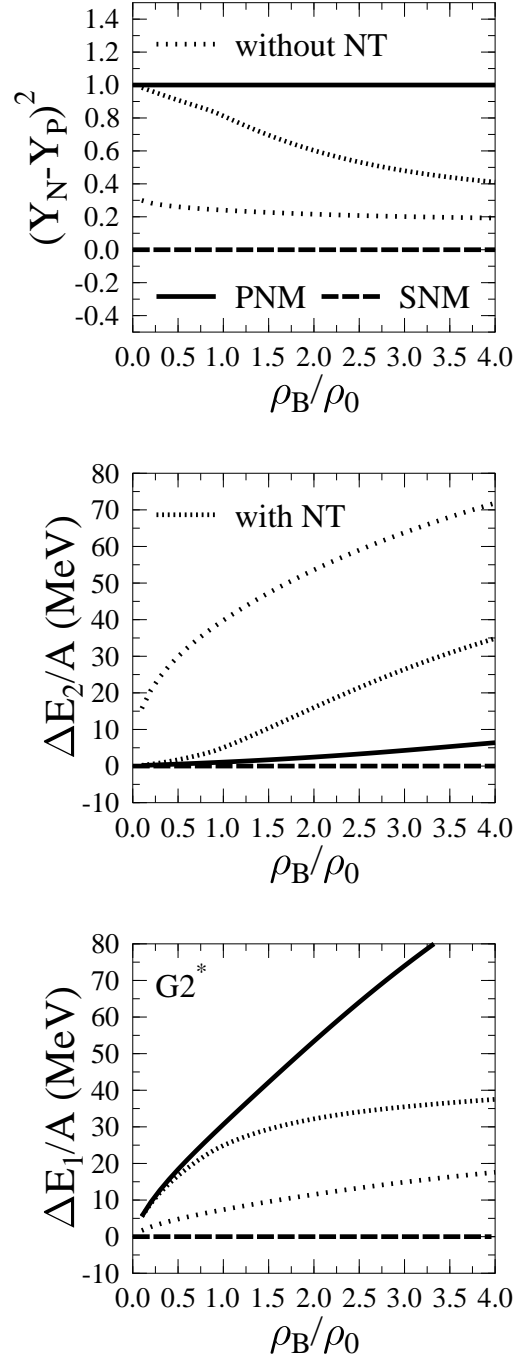
FIG. 2: $\Delta E_2/A$, $\Delta E_1/A$ and α^2 as a function of the ratio between baryon and nuclear saturation densities for matters with and without neutrino trapping (NT). The G2* parameter set and $Y_{l_e} = 0.3$ are used in obtaining these results.
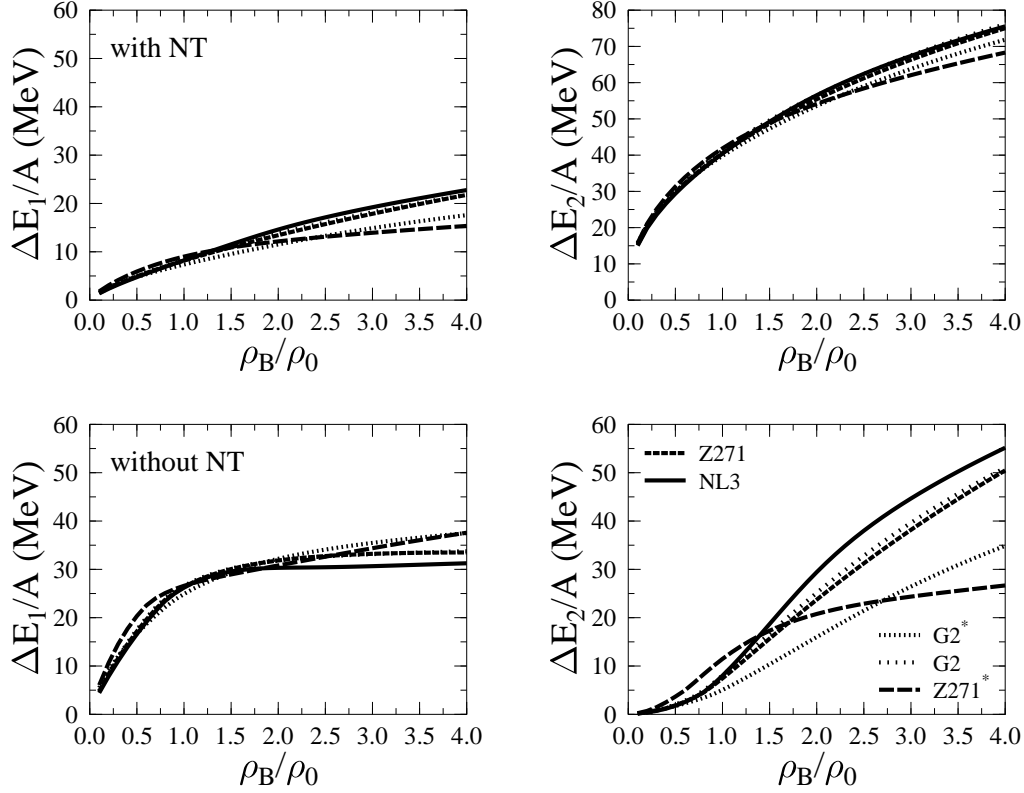
FIG. 3: $\Delta E_2/A$ and $\Delta E_1/A$ as a function of the ratio between baryon and nuclear saturation densities for matters with and without neutrino trapping (NT), obtained by using G2, G2*, Z271, Z271* and NL3 parameter sets. All curves are obtained with $Y_{l_e} = 0.3$.

α^2 on a_{sym} can be investigated by comparing Figs. 3 and 4 with Fig. 5. It is obvious that in the case of matter with neutrino trapping, correlations between $\Delta E_2/A$, $\Delta E_1/A$ and α^2 with a_{sym} at densities lower than $2\rho_0$ can not be observed, but for the neutrinoless case the opposite situation appears. For densities larger than $2\rho_0$, correlations between $\Delta E_2/A$, $\Delta E_1/A$, as well as α^2 and a_{sym} for matter with neutrino trapping is weaker than those without neutrino trapping.

Therefore, it is clear that the results displayed in Fig. 1 are caused by one reason: matter without neutrino trapping has a weak correlation with a_{sym} and especially at densities lower than $2\rho_0$, the effect is more pronounced. This effect is mainly due to the behavior of the $\Delta E_2/A$ contribution. For densities lower than $2\rho_0$, the asymmetry between protons and neutrons, which is smaller compared to the case of neutrinoless matter, also induces a correlation between $\Delta E_1/A$ and a_{sym}, whereas the role of $\Delta E_1/A$ is suppressed.
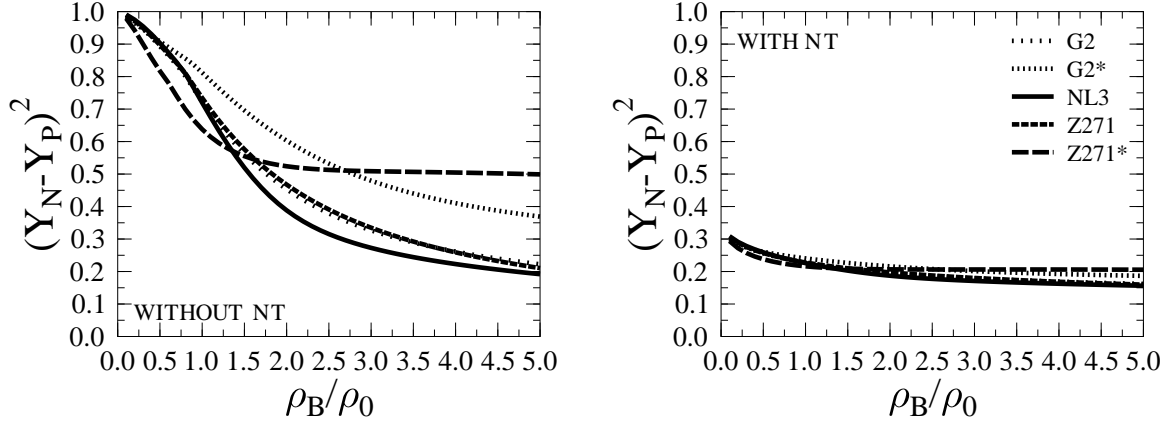
14

FIG. 4: α^2 as a function of the ratio between baryon and nuclear saturation densities for matters with and without neutrino trapping (NT). The results are obtained by using G2, G2*, Z271, Z271*, NL3 parameter sets and $Y_{l_e} = 0.3$.
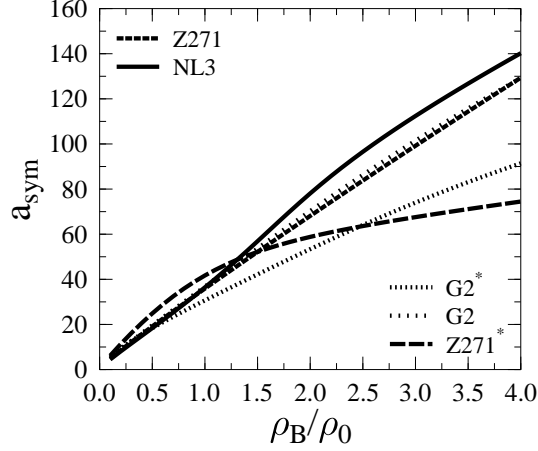

FIG. 5: Symmetry energy as a function of the ratio between baryon and nuclear saturation densities for G2, G2*, Z271, Z271* and NL3 parameter sets.

In the upper right panel of Fig. 1, Y_{ν_e} for different parameter sets are shown. It is interesting to note that NL3, Z271 and G2 parameter sets have a similar Y_{ν_e} trend but Y_{ν_e} of G2* and Z271* behaves differently. By comparing this figure with Fig. 5 we can conclude that the number of trapped neutrino correlates with the a_{sym} behavior of the models. This is due to the neutrino fraction which self consistently depends on the proton fraction (Y_p)
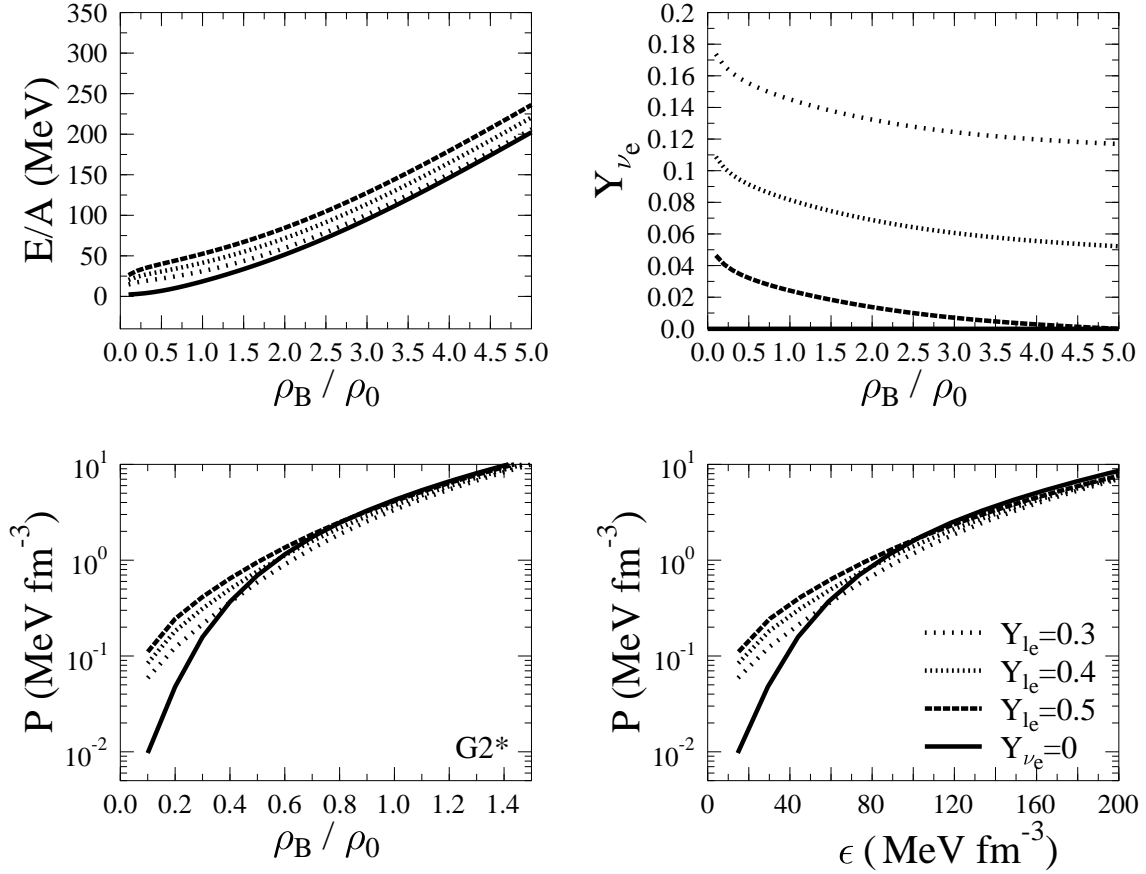
15

FIG. 6: Same as Fig. 1, but here the Y_{l_e} is varied and the G2* parameter set is used.

through the neutrality and beta equilibrium conditions, while Y_p has a correlation with a_{sym}, although the effect is quite small for this kind of matter.

To study the role of the neutrino number in the E/A and EOS using G2* parameter set, we show in the upper left panel of Fig. 6 the variation of E/A for some values of Y_{l_e} and in the lower panels the variation of their EOS. It is found that the larger the number of neutrinos in matter, the smaller the value of E/A. At low density, the EOS of matter with neutrino trapping is stiffer than that without neutrino trapping. According to Ref. [15] the reason is that the neutrino in matter shifts the threshold of muon production toward higher densities. However, for matter with neutrino trapping, the larger the number of neutrinos, the softer its EOS. At high densities the situation is opposite. Also we can see this from another point of view, i.e., by comparing the slope of dominant contributions of each case (bottom and center panels of Fig. 7). At densities less than ρ_0, the slope of $\Delta E_1/A$ for neutrinoless matter is smaller than that of $\Delta E_2/A$ for matter with neutrino trapping. In
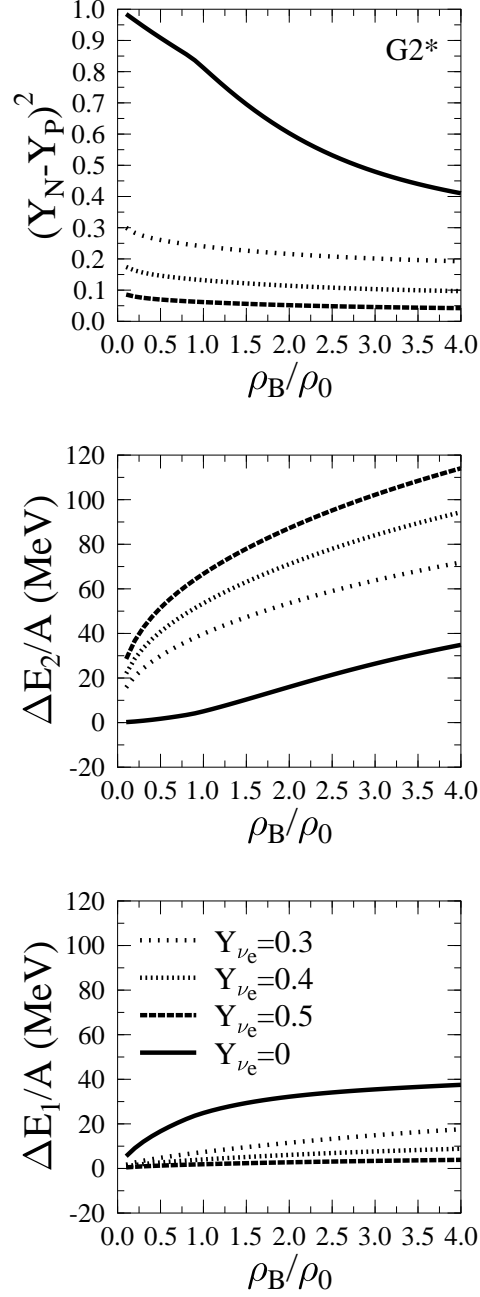
16

FIG. 7: $\Delta E_2/A$, $\Delta E_1/A$ and α as a function of the ratio between baryon density and nuclear saturation density for matters with neutrino trapping (NT) obtained by using the G2* parameter set but with varied Y_{l_e}.
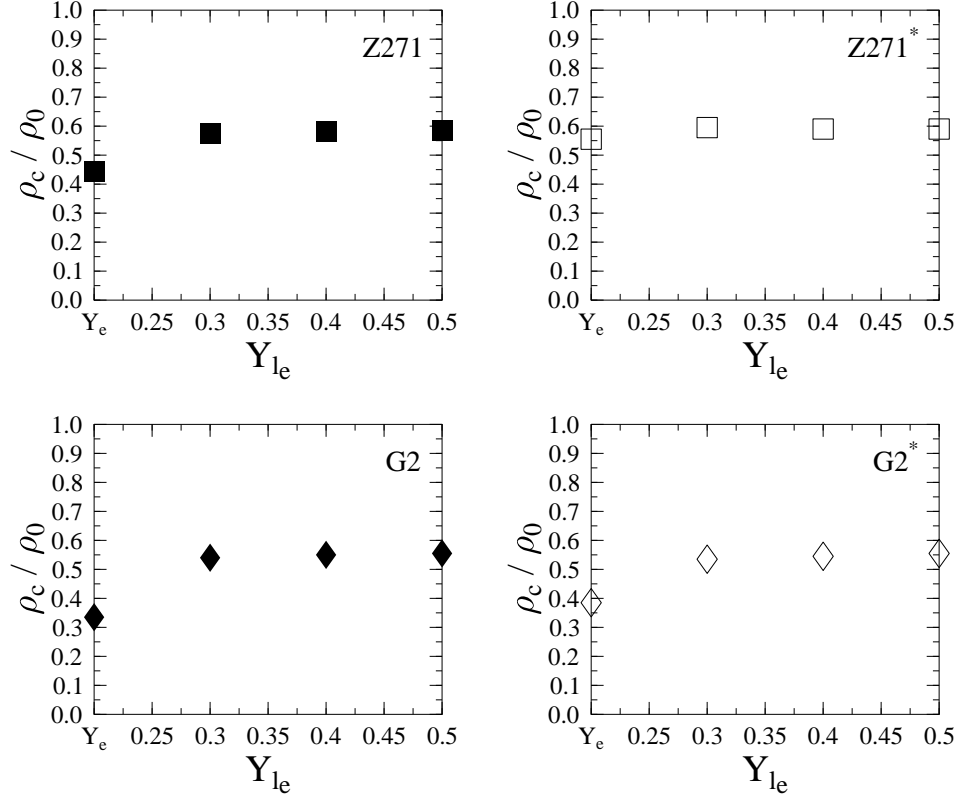
FIG. 8: Critical densities for the Z271, Z271*, G2 and G2* parameter sets as a function of the neutrino fraction in matter.

the latter, also in the same density range, even though it does not clearly visible, the slope becomes larger as Y_{l_e} becomes larger. The situation is reversed once the densities become higher than ρ_0.

The critical densities as a function of the neutrino fraction in matter are shown in Fig. 8 for the Z271 (upper left panel), Z271* (upper right panel), G2 (lower left panel), G2* (lower right panel) and in the left panel of Fig. 9 for the NL3 parameter set. Without neutrino trapping, it is obtained that $\rho_c^{G2} = 0.052 \, \text{fm}^{-3}$, $\rho_c^{G2*} = 0.060 \, \text{fm}^{-3}$, $\rho_c^{Z271} = 0.066 \, \text{fm}^{-3}$, $\rho_c^{Z271*} = 0.082 \, \text{fm}^{-3}$ and $\rho_c^{NL3} = 0.049 \, \text{fm}^{-3}$. This indicates that the critical density in the Horowitz-Piekarewicz model is larger than that of the ERMF and the NL3 parameter sets, while the standard RMF model represented by the NL3 parameter set yields the smallest value. The effects of the isovector-vector adjustment on ρ_c can be seen by comparing the panels for Z271 with Z271*, or G2 with G2*. In the Horowitz-Piekarewicz model, the variation of the ρ_c values is larger than in the ERMF one.
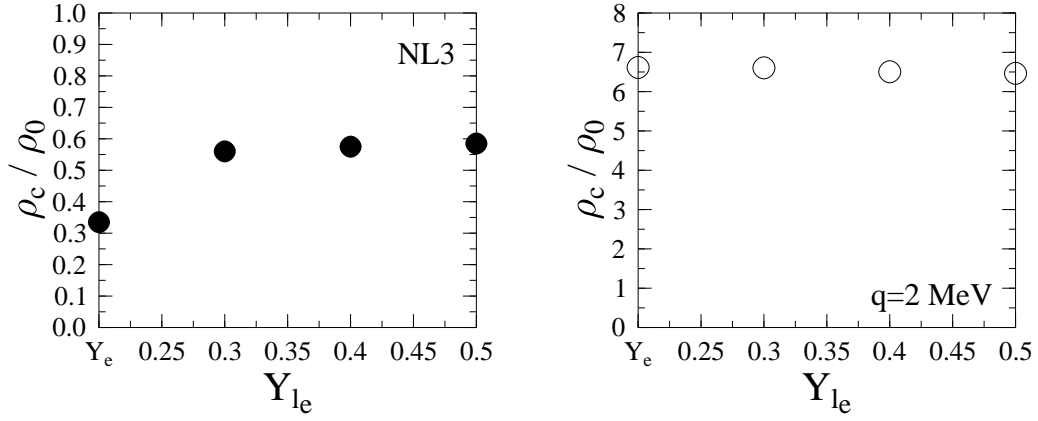
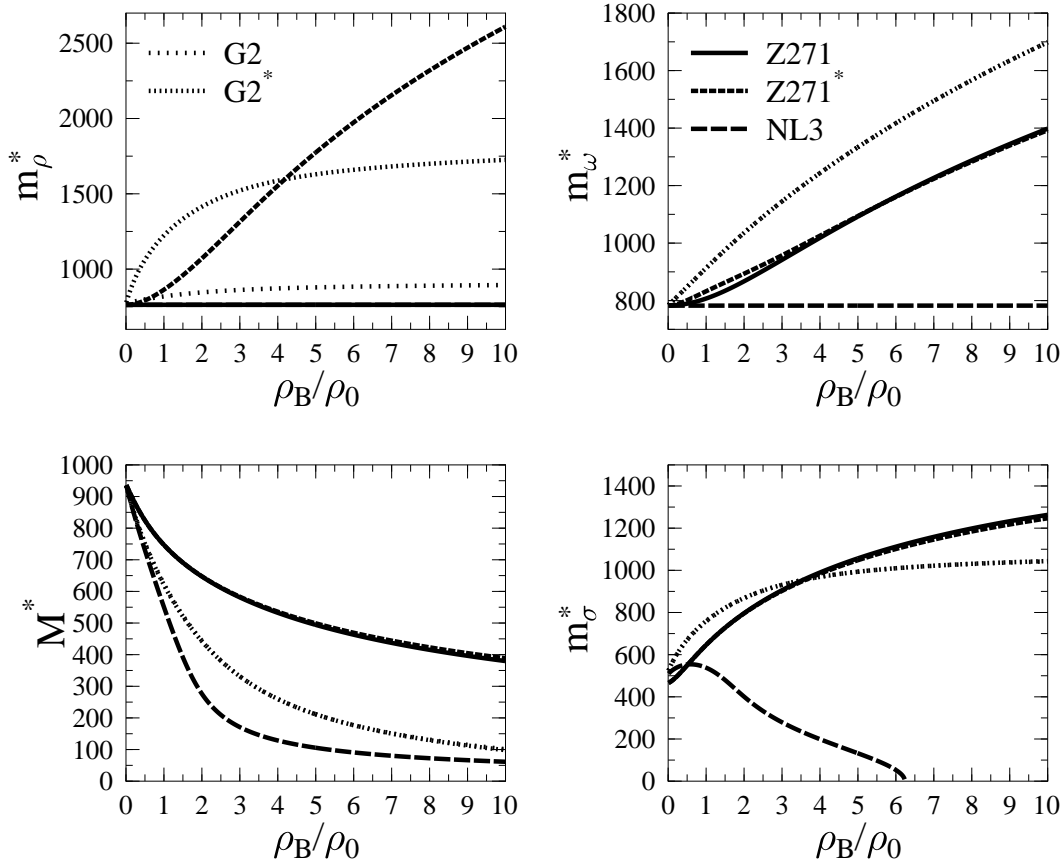FIG. 9: Same as in Fig. 8, but for the NL3 parameter set.

FIG. 10: Effective masses of nucleon, σ, ω and ρ mesons as a function of the baryon density. Note that several lines coincide.

On the other hand, with neutrino trapping we obtain, $\rho_c^{\text{G2}} = (0.084 - 0.086)$ fm^{-3}, $\rho_c^{\text{G2*}} = (0.083 - 0.086)$ fm^{-3}, $\rho_c^{\text{Z271}} = (0.085 - 0.086)$ fm^{-3}, $\rho_c^{\text{Z271*}} = (0.087 - 0.088)$ fm^{-3} and $\rho_c^{\text{NL3}} = (0.081 - 0.084)$ fm^{-3}. This indicates that for this case the value of ρ_c does not sensitively depend on the model and on the variation of the number of trapped neutrinos in matter. In general, their values are larger than those obtained in the case without neutrino trapping.

Equation (36) implies that ρ_c is determined by matter composition as well as by the effective masses of mesons and nucleons used. We know from previous results that protons and neutrons are the dominant constituents in matter composition and its behavior can be observed from the corresponding asymmetry (α) which has been discussed and shown in Figs. 4 and 6. On the other hand, the effective masses depend also on the used parameter sets (see Fig. 10). The above findings and the facts that for each parameter set $\rho_c^{\text{with NT}} < \rho_c^{\text{without NT}}$, as well as the indication that in matter with neutrino trapping and constant Y_{l_e} the critical density does not vary significantly for all parameter sets used, can be understood as the evidence of the dominant role played by the proton-neutron asymmetry in matter in determining the value of ρ_c. Furthermore, the reason that the strong dependence of ρ_c on the parameter set used in the case of matter without neutrino trapping is that the protons-neutrons asymmetry of this kind of matter has a strong correlation with the a_{sym}.

From Figs. 6, 8 and the top panel of Fig. 7 we can clearly see that the dependence of ρ_c on the number of trapped neutrinos in matter does not significantly change with respect to the variation of Y_{l_e} and the value of α^2. This result emphasizes our previous finding that there is a strong relation between ρ_c and the a_{sym}.

To show the crucial role of protons in shifting the values of ρ_c to relatively low densities, let us study the contribution of each constituent. First, the electrons, protons, and muons contributions are switched off. Then, by fixing q at 30 MeV we search for ρ_c for all parameter sets, both for trapped and untrapped neutrino cases. For all cases, we found more or less similar results, i.e., $\rho_c/\rho_0 \approx 1.7$. This value comes merely from the neutron contribution. A small difference in the neutron fraction (Y_n) for both cases has a negligible effect on the ρ_c prediction. Secondly, now in addition to the first condition, the proton contribution is switched on. Now we obtain quite different values of ρ_c, for example, in the case of G2* with $Y_{l_e} = 0.3$ we obtain $\rho_c/\rho_0 = 0.580$, and for the case without neutrino trapping we obtain $\rho_c/\rho_0 = 0.425$. Thus, it is clear that the protons shift the ρ_c values to the region with

relatively low densities. Next, the electron contribution is switched on. Then we observed that ρ_c/ρ_0 is shifted further, i.e., $\rho_c/\rho_0 = 0.430$ for $Y_{l_e} = 0.3$ and $\rho_c/\rho_0 = 0.350$ for matter without neutrino trapping. If the muons contribution is switched on, the result does not change. It happens not only in matter with neutrino trapping, but also in matter without neutrino trapping, respectively. However, these results show that the proton and electron contributions decrease the value of ρ_c in different ways for both cases and, therefore, reveal the crucial role of matter composition in determining the value of ρ_c.

In contrast to the Horowitz-Piekarewicz and ERMF models, the NL3 parameter set yields an additional instability at relatively high densities. This is shown in the right panel of Fig. 9 for the $q = 2$ MeV case, i.e., $\rho_c/\rho_0 \approx 6.5$. Even if we use q close to zero, this instability does not disappear and the ρ_c/ρ_0 value stays similar as in the $q = 2$ MeV case. Therefore, this instability is not due to the small-amplitude density fluctuations. In fact, this instability appears because the effective σ mass of the NL3 parameter set is zero at that density (as shown in the lower right panel of Fig. 10). As a consequence, the corresponding σ propagator changes the sign at this point. This fact clearly shows that additional nonlinear terms to the σ nonlinearities of the standard RMF models like in the Horowitz-Piekarewicz and ERMF ones can prevent such kind of instability to appear.

V. CONCLUSION

The effects of the different treatments in the isovector-vector sector of RMF models on the properties of matter with neutrino trapping have been studied. The effects are less significant compared to those without neutrino trapping. Different dependences of the EOS and B/A of both matters on a_{sym} are the reason behind this.

The effects of the variation of the neutrino fraction in matter on the EOS and B/A have been also discussed.

The longitudinal dielectric function of the ERMF model for matter consisting of neutrons, protons, electrons, muons, and neutrinos has been derived. The result is used to study the dynamical instability of uniform matters at low densities. The behavior of the predicted ρ_c in matter with and without neutrino trapping has been investigated. It is found that different treatments in the isovector-vector sector of RMF models yield more substantial effects in matter without neutrino trapping rather than in matter with neutrino trapping.

Moreover, for matter with neutrino trapping, the value of ρ_c does not significantly change with the variation of the models as well as with the variation of the neutrino fraction in matter. In this case, the value of ρ_c is larger for matter with neutrino trapping. These are due to the interplay between the major role of matter composition and the role of the effective masses of mesons and nucleons. It is also found that the additional nonlinear terms of Horowitz-Piekarewicz and ERMF models prevent another instability at relatively high densities to appear. This can be traced back to the effective σ mass which goes to zero when the density approaches 6.5 ρ_0 .

ACKNOWLEDGMENT

APPENDIX A: MESON PROPAGATORS

In this Appendix, simplified Dyson equations for meson propagators (only zero component of each propagator is considered) will be given. The covariant form for σ and ω couplings is given in Ref. [28]. If we define the σ, ω and ρ free propagators as

$$G_\sigma = \frac{i}{q_\mu^2 - m_\sigma^2} \qquad G_\omega^{00} = \frac{-i}{q_\mu^2 - m_\omega^2} \qquad G_\rho^{00} = \frac{-i}{q_\mu^2 - m_\rho^2}, \tag{A1}$$

the Dyson equation for the σ propagator in the absence of coupling to ω and ρ fields is obtained by considering the sum of ring diagrams, i.e.,

$$\bar{G}_\sigma = G_\sigma - iG_\sigma\Pi_{\sigma\sigma}\bar{G}_\sigma, \tag{A2}$$

from which we can obtain

$$\bar{G}_\sigma = \frac{G_\sigma}{1 + i\Pi_{\sigma\sigma}G_\sigma} = \frac{i}{q_\mu^2 - (m_\sigma^*)^2}. \tag{A3}$$

Similarly, the Dyson equations for the zero components of ω and ρ meson propagators are

$$\bar{G}_\omega^{00} = \frac{G_\omega^{00}}{1 - i\Pi_{\omega\omega}^{00}G_\omega^{00}} = \frac{-i}{q_\mu^2 - (m_\omega^*)^2}, \tag{A4}$$

22

and

$$\bar{G}_\rho^{00} = \frac{G_\rho^{00}}{1 - i\Pi_{\rho\rho}^{00}G_\rho^{00}} = \frac{-i}{q_\mu^2 - (m_\rho^*)^2}, \tag{A5}$$

where $(m_\sigma^*)^2 = (m_\sigma)^2 + \Pi_{\sigma\sigma}$, $(m_\omega^*)^2 = (m_\omega)^2 + \Pi_{\omega\omega}^{00}$, and $(m_\rho^*)^2 = (m_\rho)^2 + \Pi_{\rho\rho}^{00}$.

In the ERMF model, each meson is coupled to other mesons through the nonlinear terms. This fact further complicates the form of the full propagators. The Dyson equation for the σ propagator including the possible mixing terms becomes

$$\tilde{G}_\sigma = \bar{G}_\sigma - \bar{G}_\sigma\Pi_{\sigma\omega}^0\bar{G}_\omega^{00}\Pi_{\sigma\omega}^0\tilde{G}_\sigma - \bar{G}_\sigma\Pi_{\sigma\rho}^0\bar{G}_\rho^{00}\Pi_{\sigma\rho}^0\tilde{G}_\sigma, \tag{A6}$$

which can be written as

$$\tilde{G}_\sigma = \frac{\bar{G}_\sigma}{1 + \bar{G}_\sigma(\Pi_{\sigma\omega}^0\bar{G}_\omega^{00}\Pi_{\sigma\omega}^0 + \Pi_{\sigma\rho}^0\bar{G}_\rho^{00}\Pi_{\sigma\rho}^0)}. \tag{A7}$$

Equation (A7) can be simplified into

$$\tilde{G}_\sigma = \frac{i(q_\mu^2 - m_\omega^{*\,2})(q_\mu^2 - m_\rho^{*\,2})}{(q_\mu^2 - m_\omega^{*\,2})(q_\mu^2 - m_\rho^{*\,2})(q_\mu^2 - m_\sigma^{*\,2}) + (\Pi_{\sigma\omega}^0)^2(q_\mu^2 - m_\rho^{*\,2}) + (\Pi_{\sigma\rho}^0)^2(q_\mu^2 - m_\omega^{*\,2})}. \tag{A8}$$

Similarly, the zero component of ω and ρ meson propagators can be written as

$$\tilde{G}_\omega^{00} = \frac{-i(q_\mu^2 - m_\sigma^{*\,2})(q_\mu^2 - m_\rho^{*\,2})}{(q_\mu^2 - m_\omega^{*\,2})(q_\mu^2 - m_\rho^{*\,2})(q_\mu^2 - m_\sigma^{*\,2}) + (\Pi_{\sigma\omega}^0)^2(q_\mu^2 - m_\rho^{*\,2}) - (\Pi_{\omega\rho}^{00})^2(q_\mu^2 - m_\sigma^{*\,2})}, \tag{A9}$$

and

$$\tilde{G}_\rho^{00} = \frac{-i(q_\mu^2 - m_\sigma^{*\,2})(q_\mu^2 - m_\omega^{*\,2})}{(q_\mu^2 - m_\omega^{*\,2})(q_\mu^2 - m_\rho^{*\,2})(q_\mu^2 - m_\sigma^{*\,2}) + (\Pi_{\sigma\rho}^0)^2(q_\mu^2 - m_\omega^{*\,2}) - (\Pi_{\omega\rho}^{00})^2(q_\mu^2 - m_\sigma^{*\,2})}. \tag{A10}$$

We can also define a propagator $\tilde{G}_{\omega\sigma}^0$ which contains the sum of all diagrams that transform ω into σ, i.e.,

$$\begin{aligned}
\tilde{G}_{\omega\sigma}^0 &= -i\bar{G}_\omega^{00}\Pi_{\omega\sigma}^0\bar{G}_\sigma + i\bar{G}_\omega^{00}\Pi_{\omega\sigma}^0\bar{G}_\sigma\Pi_{\sigma\omega}^0\bar{G}_\omega^{00}\Pi_{\omega\sigma}^0\bar{G}_\sigma + \cdots \\
&\quad + i\bar{G}_\omega^{00}\Pi_{\omega\sigma}^0\bar{G}_\sigma\Pi_{\sigma\rho}^0\bar{G}_\rho^{00}\Pi_{\rho\sigma}^0\bar{G}_\sigma + \cdots + i\bar{G}_\omega^{00}\Pi_{\omega\rho}^0\bar{G}_\rho^{00}\Pi_{\rho\omega}^0\bar{G}_\omega^{00}\Pi_{\omega\sigma}^0\bar{G}_\sigma + \cdots \\
&\quad + \cdots.
\end{aligned} \tag{A11}$$

This propagator may be summed up to produce

$$\tilde{G}_{\omega\sigma}^0 = \frac{-i\bar{G}_\omega^{00}\Pi_{\omega\sigma}^0\bar{G}_\sigma}{1 + \bar{G}_\sigma\Pi_{\sigma\omega}^0\bar{G}_\omega^{00}\Pi_{\omega\sigma}^0 + \bar{G}_\sigma\Pi_{\sigma\rho}^0\bar{G}_\rho^{00}\Pi_{\rho\sigma}^0 + \bar{G}_\omega^{00}\Pi_{\omega\rho}^{00}\bar{G}_\rho^{00}\Pi_{\rho\omega}^{00}}, \tag{A12}$$

which can be simplified to

$$\tilde{G}_{\omega\sigma}^0 = \frac{-i\Pi_{\omega\sigma}^0(q_\mu^2 - m_\rho^{*\,2})}{H(q, q_0)}. \tag{A13}$$

Similarly, we can also obtain the sum of all diagrams that transform ρ into σ as

$$\tilde{G}^0_{\rho\sigma} = \frac{-i\Pi^0_{\rho\sigma}(q^2_\mu - m^{*\,2}_\omega)}{H(q, q_0)}, \tag{A14}$$

and that transform ρ into ω as

$$\tilde{G}^{00}_{\rho\omega} = \frac{i\Pi^{00}_{\rho\omega}(q^2_\mu - m^{*\,2}_\sigma)}{H(q, q_0)}, \tag{A15}$$

where

$$H(q, q_0) = (q^2_\mu - m^{*\,2}_\omega)(q^2_\mu - m^{*\,2}_\rho)(q^2_\mu - m^{*\,2}_\sigma) + (\Pi^0_{\sigma\omega})^2(q^2_\mu - m^{*\,2}_\rho) + (\Pi^0_{\sigma\rho})^2(q^2_\mu - m^{*\,2}_\omega)$$

$$- (\Pi^{00}_{\omega\rho})^2(q^2_\mu - m^{*\,2}_\sigma). \tag{A16}$$

Equations (28) - (33) are special cases of Eqs. (A8 - A10, A13, A14, A15), i.e. by taking the limit of $q_0 \to 0$ and inserting the proper mesons coupling constants in the latter.

APPENDIX B: EXPLICIT FORM OF THE LONGITUDINAL DIELECTRIC FUNCTION

In this Appendix, the explicit form of the longitudinal dielectric function $\epsilon_L = [1 - D_L(q)\Pi_L(q, q_0 = 0)]$ is provided. If we define the matrix ϵ_L as

$$\epsilon_L = \begin{pmatrix} A_1 & B_1 & D_1 & E_1 & F_1 \\ A_2 & B_2 & D_2 & E_2 & F_2 \\ A_4 & B_4 & D_4 & E_4 & F_4 \\ A_5 & B_5 & D_5 & E_5 & F_5 \\ A_6 & B_6 & D_6 & E_6 & F_6 \end{pmatrix}, \tag{B1}$$

then the contents of each component of the matrix in Eq. (B1) are

$$\begin{aligned}
A_1 &= 1 - d_g\Pi^e_{00}, & A_2 &= -d_g\Pi^e_{00}, & A_4 &= 0, \\
B_1 &= -d_g\Pi^\mu_{00}, & B_2 &= 1 - d_g\Pi^\mu_{00}, & B_4 &= 0, \\
D_1 &= d_g\Pi^p_m, & D_2 &= d_g\Pi^p_m, & D_4 &= 1 + d_s\Pi_s - d^+_{sv\rho}\Pi^p_m - d^-_{sv\rho}\Pi^n_m, \\
E_1 &= d_g\Pi^p_{00}, & E_2 &= d_g\Pi^p_{00}, & E_4 &= d_s\Pi^p_m - d^+_{sv\rho}\Pi^p_{00}, \\
F_1 &= 0, & F_2 &= 0, & F_4 &= d_s\Pi^n_m - d^-_{sv\rho}\Pi^n_{00},
\end{aligned} \tag{B2}$$

and

$$
\begin{aligned}
&A_5 = d_g \Pi_{00}^e, &&A_6 = 0, \\
&B_5 = d_g \Pi_{00}^\mu, &&B_6 = 0, \\
&D_5 = -d_{sv\rho}^+ \Pi_s - d_{33} \Pi_m^p - d_{v\rho}^- \Pi_m^n, &&D_6 = -d_{sv\rho}^- \Pi_s - d_{v\rho}^- \Pi_m^p - d_{44} \Pi_m^n, &&\text{(B3)} \\
&E_5 = 1 - d_{sv\rho}^+ \Pi_m^p - d_{33} \Pi_{00}^p, &&E_6 = -d_{sv\rho}^- \Pi_m^p - d_{v\rho}^- \Pi_{00}^p, \\
&F_5 = -d_{sv\rho}^+ \Pi_m^n - d_{v\rho}^- \Pi_{00}^n, &&F_6 = 1 - d_{sv\rho}^- \Pi_m^n - d_{44} \Pi_{00}^n.
\end{aligned}
$$

[1] C.J. Pethick, D. G. Ravenhall, and C. P. Lorenz, Nucl. Phys. A **584**, 675 (1995).

[2] F. Douchin, and P. Haensel, Phys. Lett. B **485**, 107 (2001).

[3] J. Carriere, C. J. Horowitz, and J. Piekarewicz, Astrophys. J **593**, 463 (2003).

[4] C. J. Horowitz, and J. Piekarewicz, Phys. Rev. Lett **86**, 5647 (2001).

[5] S. S. Avancini, L. Brito, D. P. Menezes, and C. Providência, Phys. Rev. C **71**, 044323 (2005).

[6] C. Providência, L. Brito, S. S. Avancini, D. P. Menezes, and Ph. Chomaz, Phys. Rev. C **73**, 025805 (2006).

[7] C. J. Horowitz, and K. Wehberger, Nucl. Phys. A **531**, 665 (1991); *ibid.* Phys. Lett. B **266**, 236 (1991).

[8] R. J. Furnstahl, B. D Serot, and H. B. Tang, Nucl. Phys. A **598**, 539 (1996); Nucl. Phys. A **615**, 441 (1997).

[9] T. Sil, S. K. Patra, B. K. Sharma, M. Centelles, and X. Vinãs, *Focus on Quantum Field Theory*, Edited by O. Kovras (Nova Science Publishers, Inc, New York, 2005).

[10] B. D. Serot, and J .D. Walecka, Int. J. Mod. Phys. E **6**, 515 (1997); and references therein.

[11] A. Sulaksono, P. T. P. Hutauruk, and T. Mart, Phys. Rev. C **72**, 065801 (2005).

[12] M. Prakash, I. Bombaci, M. Prakash, P. J. Ellis, J. M. Lattimer, and R. Knorren, Phys. Rep. **280**, 1 (1997).

[13] I. Vidaña, I. Bombaci, A. Polls and A. Ramos, Astron. Astrophys **399**, 687 (2003).

[14] Guo Hua, Chen Yanjun, Liu Bo, Zhao Qi, and Liu Yuxin, Phys. Rev. C **68**, 035803 (2003).

[15] M. Chiapparini, H. Rodrigues, and S.B. Duarte, Phys. Rev. C **54**, 936 (1996).

[16] I. Bednarek, and R. Manka, Phys. Rev. C **73**, 045804 (2006).

[17] H. Shen, H. Toki, K. Oyamatsu, and K. Sumiyoshi, Nucl. Phys. A **637**, 435 (1998).

[18] G. Watanabe, K. Iida, and K. Sato, Nucl. Phys. A **687**, 512 (2001).

[19] G.A. Lalazissis, J. Konig, and P. Ring, Phys. Rev. C **55**, 540 (1997).

[20] A. Sulaksono, C. K. Williams, P. T. P. Hutauruk, and T. Mart, Phys. Rev. C **73**, 025803 (2006).

[21] P.-G. Reinhard, Rep. Prog. Phys **52**, 439 (1989); and references therein.

[22] P. Ring, Prog. Part. Nucl. Phys **37**, 193 (1996); and references therein.

[23] P. Wang, Phys. Rev. C **61**, 054904 (2000).

[24] G. Shen, J. Li, G. C. Hillhouse, and J. Meng, Phys. Rev. C **71**, 015802 (2005).

[25] A. E. L. Dieperink, Y. Dewulf, D. Van Neck, M. Waroquier, and V. Rodin, Phys. Rev. C **68**, 064307 (2003).

[26] A. W. Steiner, nucl-th/0607040 (2006).

[27] C. J. Horowitz, and M. A. Pérez-García, Phys. Rev. C **68**, 025803 (2003).

[28] L.S. Celenza, A. Pantziris, and C. M. Shakin, Phys. Rev. C **45**, 205 (1992).